Biophys Rev (2017) 9:729–745
DOI 10.1007/s12551-017-0323-1

REVIEW

Experimental and theoretical studies of emodin interacting with a lipid bilayer of DMPC

Antonio R. da Cunha[1,2] · **Evandro L. Duarte**[2] · **Hubert Stassen**[3] · **M. Teresa Lamy**[2] · **Kaline Coutinho**[2]

Received: 7 June 2017 / Accepted: 29 August 2017 / Published online: 22 September 2017

Abstract Emodin is one of the most abundant anthraquinone derivatives found in nature. It is the active principle of some traditional herbal medicines with known biological activities. In this work, we combined experimental and theoretical studies to reveal information about location, orientation, interaction and perturbing effects of Emodin on lipid bilayers, where we have taken into account the neutral form of the Emodin (EMH) and its anionic/deprotonated form (EM^-). Using both UV/Visible spectrophotometric techniques and molecular dynamics (MD) simulations, we showed that both EMH and EM^- are located in a lipid membrane. Additionally, using MD simulations, we revealed that both forms of Emodin are very close to glycerol groups of the lipid molecules, with the EMH inserted more deeply into the bilayer and more disoriented relative to the normal of the membrane when compared with the EM^-, which is more exposed to interfacial water. Analysis of several structural properties of acyl chains of the lipids in a hydrated pure DMPC bilayer and in the presence of Emodin revealed that both EMH and EM^- affect the lipid bilayer, resulting in a remarkable disorder of the bilayer in the vicinity of the Emodin. However, the disorder caused by EMH is weaker than that caused by EM^-. Our results suggest that these disorders caused by Emodin might lead to distinct effects on lipid bilayers including its disruption which are reported in the literature.

Keywords Emodin · Phospholipid bilayer · Molecular dynamic simulation · UV/Visible spectroscopy

This article is part of a Special Issue on 'Latin America' edited by Pietro Ciancaglini and Rosangela Itri.

Electronic supplementary material The online version of this article (https://doi.org/10.1007/s12551-017-0323-1) contains supplementary material, which is available to authorized users.

✉ Kaline Coutinho
kaline@if.usp.br

Antonio R. da Cunha
cunha.antonio@ufma.br

Evandro L. Duarte
elduarte@if.usp.br

Hubert Stassen
gullit@iq.ufrgs.br

M. Teresa Lamy
mtlamy@if.usp.br

[1] Universidade Federal do Maranhão, UFMA, Campus Balsas, Maranhão 06500-000, Brazil

[2] Instituto de Física da Universidade de São Paulo, 05508-090, Cidade Universitária, São Paulo, Brazil

[3] Grupo de Química Teórica, Instituto de Química, UFRGS, Av. Bento Gonçalves 9500, Porto Alegre 91540-000, Brazil

Introduction

The interaction of a pharmacophore with cell membranes is a topic of great interest in biology and pharmacology due to the possible relevance in the pathway of action (Apostolova et al. 2003; Duarte et al. 2008; Peetla et al. 2009). There are several molecular features that govern the behavior of a drug in cell membranes such as size, shape, solubility, hydrophilicity, lipophilicity, and pK_a, among others. Previously, many authors have reported studies of the interaction of drugs and membrane models with experimental technics (Nunes et al. 2011; Lucio et al. 2009; Fuchs et al. 1990) and molecular dynamic (MD) simulations (Robinson et al. 1995; Gabdouline et al. 1996; Smondyrev and Berkowitz 1999, 2001; Hofsäß et al. 2003; Pereira et al. 2004; Falck et al. 2006; Högberg et al. 2007; Seddon et al. 2009; Sirk et al. 2009; Boggara and

Krishnamoorti 2010; Witzke et al. 2010; Orsi and Essex 2010, Koukoulitsa et al. 2011; Nitschke et al. 2012; Poger and Mark 2013; Loverde 2014; Jalili and Saeedi 2016). In particular, studies based on drug partitioning in lipid bilayers and the thermodynamics of drug/lipid interaction have great importance in understanding the reaction mechanisms of antitumor drugs and to design new cell membrane-targeted drugs (Boggara and Krishnamoorti 2010; Jendrossek and Handrick 2003; Goldstein et al. 2011; Choi et al. 2013).

Several drugs and molecules of biological interest that interact with the cell membrane in their acting or metabolic mechanism, respectively, have in their chemical structure hydrophilic and lipophilic groups, such as Aspirin, Ibuprofen, Lidocaine, Alprenolol, Atenolol, Pindolol, and many others. For these kinds of molecules, it is important to identify their interaction with the molecules that compose the membranes and try to understand the roles of the hydrophilic and lipophilic groups. In this direction, the MD simulations are an useful tool and can identify the location of the drug in the membrane models (Boggara and Krishnamoorti 2010; Loverde 2014; Högberg et al. 2007; Orsi and Essex 2010). It has been adopted in theoretical studies of biological membrane models (Tieleman et al. 1997; Poger and Mark 2010, 2012) and partitioning and interaction of drugs in lipid bilayers (Fuchs et al. 1990; Omote and Al-Shawi 2006; MacCallum and Tieleman 2006; Bemporad et al. 2004). Indeed, MD simulations have contributed significantly to the understanding of the structure, dynamics and effects of biological molecules in lipid bilayers (Seydel and Wiese 2002; Xiang and Anderson 2006; Yamamoto et al. 2012; Rissanen et al. 2014; Almeida et al. 2017). However, due to the variety of classical force fields available, it is important to compare the results obtained from the simulations with the experimental data to validate the simulation force field and protocols. An example of experimental technique that can be used to obtain valuable information about the thermodynamic signatures (enthalpy, entropy, affinity and stoichiometry) of drugs with biological systems, like proteins and membranes, is the isothermal titration calorimetry (ITC) (Rajarathnam and Rösgen 2014).

In this work, we report a study of the location, interaction and perturbing effects of Emodin on the model membrane composed by 1,2-dimiristoyl-sn-glycero-3-phosphocholine (DMPC) using experimental and theoretical techniques. Using UV/Visible spectrophotometry, we identify the location of Emodin in its neutral (EMH) and deprotonated form (EM^-) in the DMPC bilayer, comparing the halochromic and solvatochromic effects on the absorption spectra in solution. Additionally, we performed MD simulations of both EMH and EM^- species in fully hydrated DMPC bilayer to elucidate in atomic detail the structural properties and interaction of these species in lipid membranes and its preferred location and orientation across the lipid environment. From the experimental and theoretical point of view, the location and the effect of EMH are compared with those obtained for EM^- in the DMPC bilayer. It is shown that both EMH and EM^- exhibit similar behavior in the bilayer, whereas both species are located in the head group region of the bilayer, remaining close to glycerol groups of the lipids. However, we found that the EMH is more deeply inserted in the bilayer than EM^-. Furthermore, analysis of several structural properties, such as area per lipid, electron density profile, radial distribution functions, hydrogen bonds distribution and order parameters profiles of the acyl chains of the lipids in a hydrated pure DMPC bilayer and in Emodin-containing bilayers revealed that both EMH and EM^- affect the lipid bilayer, resulting in remarkable disorders of the membrane in the vicinity of the Emodin. However, the effect of EM^- is slightly stronger than that of EMH.

Emodin (1,3,8-trihydroxy-6-methyl-9,10-anthraquinone, Fig. 1) is a natural anthraquinone derivative extracted from herbal medicines such as Polygonaceae, Rhamnaceae and Cassieae, which are traditionally used in Chinese medicine (Thomson 1987; Izhaki 2002; Dong et al. 2016). This anthraquinone has been reported to have biological activity, such as anticancer (Chen et al. 2002; Srinivas et al. 2003; Chan et al. 1993), antibacterial (Anke et al. 1980; To 1984; Wang and Chung 1997), antiviral (Barnard et al. 1992; Kawai et al. 1984), anti-inflammatory (Kumar et al. 1998; Kuo et al. 2001), diuretic and vasorelaxant effects (Koyama et al. 1988; Zhou and Chen 1988; Huang et al. 1991). It is widely accepted that these actions take place via the inhibition of protein kinase activities (Francke et al. 1978; Hsiang and Ho 2008; Zhang and Hung 1996; Jayasuriya et al. 1992). Recently, a review has discussed its pharmacology, toxicity and pharmacokinetics (Dong et al. 2016).

In previous studies, UV/Visible absorption and fluorescence spectroscopy have been applied as analytical tools to study the interaction of Emodin with solvents (Pal and Jana 1993; Nguyen et al. 2008; Sevilla et al. 2009; da Cunha et al. 2014), with biological environments like human serum albumin (HSA) (Fabriciova et al. 2004; Vargas et al. 2004), DNA (Wang et al. 2006; Saito et al. 2012; Bi et al. 2008), phospholipid bilayer (Alves et al. 2004) and with other environments

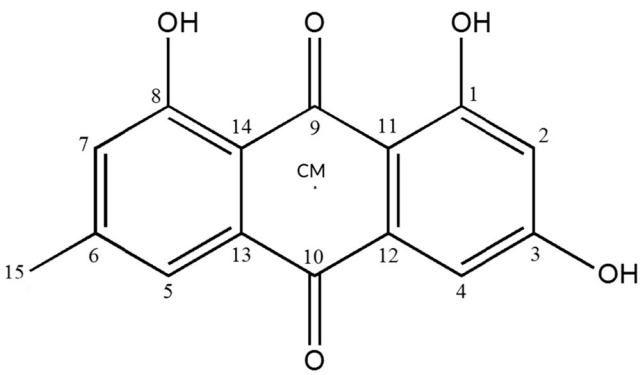

Fig. 1 Chemical structure and atomic numbering of Emodin in its neutral form (EMH)

like porous silicon (Hernandez et al. 2012), silver nanoparticles (Sevilla et al. 2009, 2010) and some metal ions (Pal and Jana 1993). It is known that Emodin exhibits in solution remarkable halochromic effects in absorption (Pal and Jana 1993; Nguyen et al. 2008; da Cunha et al. 2014) and emission spectra (Sevilla et al. 2009, 2010; Ghomi 2012). Thus, the first absorption band and the emission band are shifted by several tens of wavenumbers when the pH of the solution changes from acidic to alkaline. In a recent work (da Cunha et al. 2014), we discussed the absorption spectra of this molecule in different solvents where we showed that, in acidic aqueous solution and in common organic solvents, the main band has its maximum located around 440 nm and shows low sensitivity due to the medium. In alkaline solutions, this broad band is red-shifted, with absorption maxima, λ_{max}, varying between 520 nm (water) and 555 nm (DMSO) depending on the solvent. It is known that these effects are a consequence of the deprotonation process of Emodin in solution ($EMH \rightarrow EM^- + H^+$). Thus, the neutral form of the Emodin (EMH) is yellow, insoluble in water, but soluble in most organic solvents, and with no solvatochromism dependence on the solvent polarity. On the other hand, the anionic/deprotonated form (EM^-) is red, soluble in water and in organic solvents, and exhibits solvatochromic effects in absorption spectra. Based on quantum mechanical calculations, we previously revealed (da Cunha et al. 2014) that the first deprotonation takes place at the hydroxyl substitution of carbon 3 (see Fig. 1). Additionally, using the UV/Visible spectrophotometric titration technique, we reported the pK_{a1} of Emodin in water at 8.0 ± 0.1.

From experimental and theoretical points of view, some authors have studied the Emodin in solution by spectroscopic techniques, quantum mechanical calculations and molecular simulations elucidating many structural and electronic properties of this molecule (Pal and Jana 1993; Nguyen et al. 2008; da Cunha et al. 2014; Marković and Manojlović 2009). However, only one study has investigated the properties of neutral Emodin in phospholipid membranes (Alves et al. 2004). Much of what is known about the behavior of Emodin in lipid membranes comes from an experimental study by Alves et al. (2004), reporting an extensive and detailed spectroscopic and thermoanalytical study of its neutral form in model membranes. In this work, the authors used fluorescence spectroscopy to determine a phospholipid/water partition coefficient, K_p of $(14 \pm 2) \times 10^3$ for neutral Emodin in the DMPC bilayer, indicating that this molecule exhibits high affinity for phospholipid membranes. They also used differential scanning calorimetry (DSC) and fluorescence spectroscopy to infer the location of neutral Emodin in the bilayer, and found that this molecule seems to be located in the head group region by affecting DMPC membranes. In addition, other experimental studies have shown that the Emodin may also confer additional effects on cancer cell membranes like cell migration (Huang et al. 2005), invasion (Huang et al. 2004) and cell adhesion (Huang et al. 2006). However, despite these studies, little is known about the behavior of the deprotonated form in cell membranes. Further, the mechanism involved in the effect of both EMH and EM^- on the lipid bilayer at a molecular level remains unknown.

Experimental details

Materials

Emodin (C15H10O5; Fig.1), hydrochloric acid (HCl) and sodium hydroxide (NaOH), sodium biphosphate monohydrate (NaH2PO4.H2O), sodium phosphate dibasic heptahydrate (Na2HPO4.7H2O), sodium bicarbonate (NaHCO3), sodium carbonate (Na2CO3) and solvents were purchased from Sigma-Aldrich (St. Louis, MO, USA) and have been used without further purification. DMPC (1,2-dimiristoyl-sn-glycero-3-phosphocholine) was obtained from Avanti Polar Lipids (Birmingham, AL, USA), and used without further purification. Milli-Q water was used throughout.

Sample preparation

Binary mixtures of DMPC Emodin (2 mol% Emodin/DMPC, hence 50 lipids per Emodin molecule) were dissolved in chloroform. Next, this mixture was separated in different glass vials and dried under a stream of N_2, forming lipid films at the bottom of the vials. The films were left under reduced pressure for a minimum of 2 h to remove all traces of organic solvents. Then, two lipid dispersions containing Emodin were prepared with pH = 6.0 and pH = 10.0. These pH values were selected to guarantee that the Emodin are in the neutral/protonated form, EMH, and anionic/deprotonated form, EM^-, considering the pKa = 8.0 ± 0.1 of Emodin in water (da Cunha et al. 2014). The lipid dispersions containing predominantly EMH at pH = 6.0 were produced by the addition of sodium biphosphate/phosphate buffer obtained by mixing 10 mM $NaH_2PO_4.H_2O$ aqueous solution with 10 mM $Na_2HPO_4.7H_2O$. Similarly, the lipid dispersions containing predominantly EM^- at pH = 10.0 were produced by the addition of sodium bicarbonate/carbonate buffer obtained from the mixture of 10 mM $NaHCO_3$ aqueous solution with 10 mM Na_2CO_3. The final lipid concentration was at 1 mM. After hydration, the lipid dispersions were vortexed for ~2 min followed by extrusions, 31 times, through polycarbonate filters (mini-extruder by Avanti Polar Lipids, 19-mm membranes with 100-nm pores, from Whatman, Maidstone, Kent, UK), at a temperature above the lipid phase transition of DMPC (T = 23 °C) (Marsh 1990; Heimburg 2007). This procedure was performed in order to obtain less turbid samples, with large unilamellar vesicles (LUV).

UV/visible spectrophotometric

Absorbance measurements were performed with a Varian Cary 50 UV-Vis Spectrophotometer at a temperature of 30 °C. Samples were placed in quartz cuvettes with a 10-mm optical pathway. All spectral curves were subtracted by baselines obtained from samples without Emodin. The samples were homogenized by strongly vortexing immediately before each measurement and its pH was measured with a Mettler Toledo pH-meter.

Theoretical details

Simulated systems

We performed molecular dynamic simulations of Emodin in aqueous solution and in hydrated DMPC bilayer. The simulated system are: (1) water + EMH or water + EM^- with two systems consisting of either EMH or EM^- species solvated by 500 water molecules; (2) pure-DMPC with one lipid bilayer consisting of 338 DMPC molecules hydrated by 18,786 water molecules; and (3) DMPC + EMH or DMPC + EM^- with four systems with one hydrated lipid bilayer containing one Emodin (either EMH or EM^-) inserted in two initial positions: (3a) the Emodin inserted in the center of bilayer, as shown in Fig. 2a, with the lipid bilayer consisting of 314 DMPC with either EMH or EM^-, hydrated by 18,785 water molecules; and (3b) the Emodin inserted in the top of the bilayer, as shown in Fig. 2b, with the lipid bilayer consisting of 319 DMPC with either EMH or EM^-, hydrated by 18,773 water molecules. For these four systems,the starting orientations of Emodin in the lipid bilayer were chosen with its long axis aligned with the bilayer normal axis (z-axis), with the methyl group C15 point to the middle of the bilayer. This orientation was selected because this it the most hydrophobic region of the molecule and it could favor the insertion of the Emodin in the bilayer.

The pure-DMPC system was constructed replicating the lipid molecule on a 13 × 13 grid on up-and-down monolayers followed by hydration with 9393 water molecules in each lipid monolayer, which correspond to approximately 55 H_2O per lipid. To construct the systems DMPC + EMH and DMPC + EM^-, we started from an equilibrated configuration of the pure-DMPC system obtained from a simulation of 150 ns, as described in the next section. To add Emodin in the pure-DMPC bilayer, we inserted either EMH or EM^- removing those molecules, which overlap with Emodin. For each system containing Emodin, we generated two different initial configurations: inserting it in the center of the pure-DMPC bilayer (removing 24 lipids and 1 water molecule) and inserting it at the top of the pure-DMPC bilayer (removing 19 lipids and 13 water molecule).

Computational details of the simulations

Molecular dynamic simulations were carried out for EMH and EM^- in aqueous solution and in the hydrated lipid bilayer, using standard procedures in the isothermal–isobaric NPT ensemble. The temperature of the systems was maintained constant at 30 °C, using the Berendsen thermostat (Berendsen et al. 1984), with a coupling constant of 0.1 ps. This temperature is above the phase transition temperature of DMPC (T = 296 K) (Marsh 1990; Heimburg 2007). The pressure was kept at 1 bar by coupling to an isotropic pressure bath in solution and a semi-isotropic pressure bath in systems with the bilayer by Berendsen pressure coupling (Berendsen et al. 1984), using an isothermal compressibility of 4.6×10^{-5} bar^{-1} and a coupling constant of 1 ps. The integration of the equations of motion was performed using the leap-frog algorithm (Cuendet and van Gunsteren 2007), with a time step of 2 fs. All the bond lengths within these molecules were constrained using the LINCS algorithm (Hess et al. 1997). For the water molecules, we used the SPC model (Berendsen et al. 1981) and the bond and angles were constrained by the SETTLE algorithm (Miyamoto and Kollman 1992). The non-bonded interactions within the cut-off of 1.4 nm were calculated at every step. Long-range corrections of the electrostatic interactions beyond the cut-off were calculated using the Particle Mesh Ewald (PME) method (Essmann et al. 1995). The united atom option of GROMOS 54a7 force field (Huang et al. 2011; Schmid et al. 2011; Poger et al. 2010) was used to calculate the intermolecular and intramolecular interactions for all systems. The DMPC topology was constructed from the Automated Topology Builder (ATB) and repository (Malde et al. 2011). The optimized structure of EMH and EM^- were obtained though quantum mechanical (QM) calculations with density functional theory (DFT) (Parr and Yang 1994) using the B3LYP exchange–correlation functional (Becke 1993; Imamura et al. 2007) and the Pople basis set functions, 6–311++G(d,p) (Ditchfield et al. 1971). The charge sets for EMH and EM^- were calculated using the electrostatic potential fit CHELPG procedure (Breneman and Wiberg 1990) at the B3LYP/6–311++G(d,p) level of theory, in vacuum (charge set denoted as CS0) and also in an aqueous solution environment (charge set denoted as CS1) described by the polarizable continuum model (PCM) (Miertus et al. 1981). The atomic charges CS0 and CS1 of EMH and EM^- used in this work are shown in Supplementary Material and will be discussed later. Each system composed by the Emodin–DMPC bilayer was initialized with a thermalized pure-DMPC bilayer conformation obtained after 150 ns of simulation and with the Emodin in two initial positions (inside the bilayer and in the top of the bilayer; see Fig. 2). These two initial setup for EMH and EM^- were simulate for 200 ns and all the collected data were stored at intervals of 2 ps. Regardless of the initial position of both forms of Emodin, the same results were obtained.

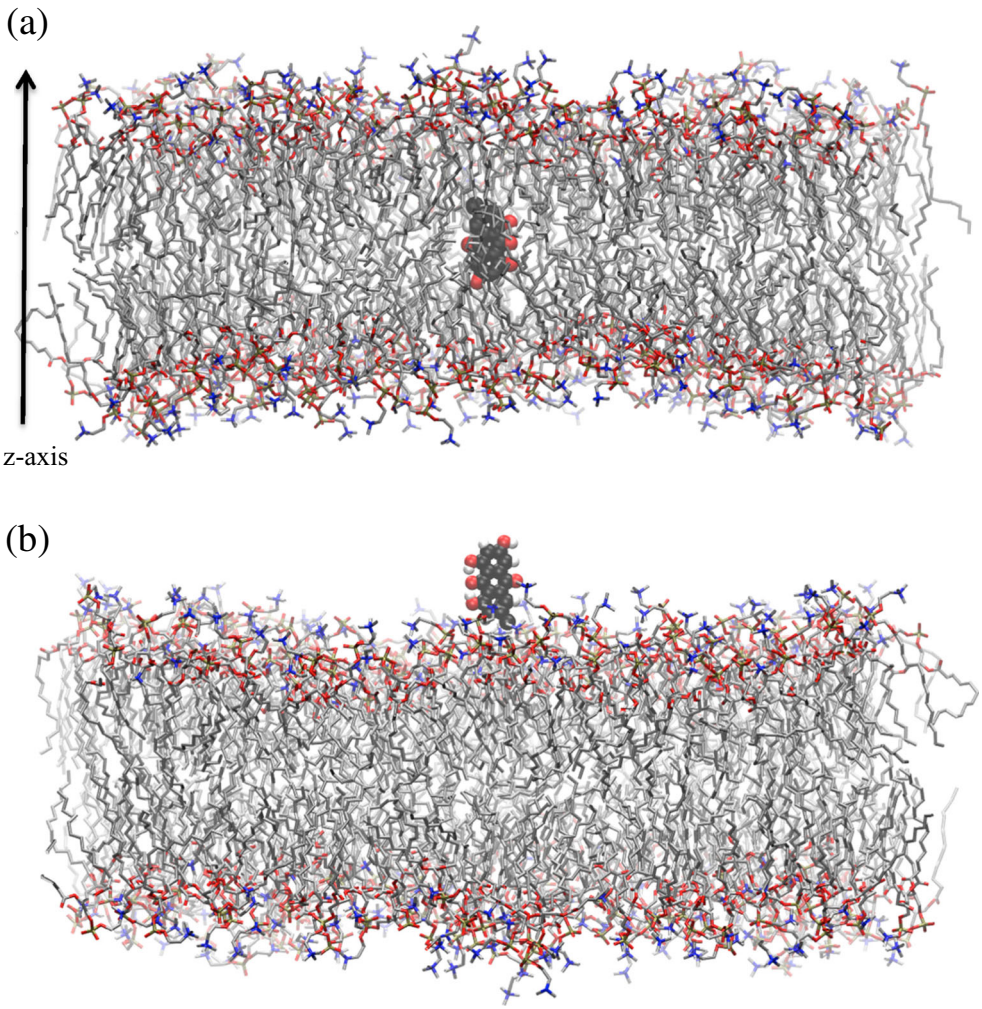

Fig. 2 Initial configurations of the simulations of both forms of Emodin (EMH or EM⁻) in the lipid bilayers. (**a**) the Emodin is inserted in the center of the bilayer and (**b**) the Emodin is inserted in the top

However, for simplicity, only the results obtained with the Emodin initially in the top of the bilayer are presented in "Theoretical Results". Equilibration was characterized by monitoring the time evolution of energy terms and the area per lipid for systems consisting of the lipid bilayer (see Supplementary Material). As will be shown in the next section, all the systems achieved equilibrium within 50 ns, and, therefore, we used the last 150 ns of the simulations for the data analysis. All simulations were performed using the GROMACS software, v.4.5.4 (Spoel et al. 2005), and all QM calculations were performed with the Gaussian 03 program, v.C.01 (Frisch et al. 2004).

Experimental results

To investigate the location of the Emodin in the lipid bilayer, we studied the halochromism and solvatochromism of this molecule in aqueous media and lipid dispersions. It is important to point out that DMPC is neutral and zwitterionic at both pH 6.0 and 10. Figure 3(a) shows the UV-Vis absorption spectra of Emodin in lipid and aqueous (buffer solutions) environments at two different pH values (pH = 6.0 and pH = 10.0, corresponding to the conditions where Emodin exists predominantly in the neutral (EMH) and anionic/deprotonated form (EM⁻), respectively. The optical absorbance curve of EMH in the lipid environment exhibits an intense absorption band centered at 446 nm, which is more intense than the absorption band of EMH in buffer solution of pH = 6.0. In this buffer, this band is weak and broad with a maximum around of the same wavelength (446 nm). As discussed before (da Cunha et al. 2014) for pH < 7.7, Emodin aggregates in aqueous solution, precipitating very quickly, and its absorption spectrum presents light scattering due the presence of these aggregates. Therefore, the observed weak and broad band on the spectrum of EMH in buffer solution of pH = 6.0 is due to the Emodin aggregation in acidic aqueous solution. Interestingly, the spectrum of EMH in lipid dispersions does not exhibit a scattering profile, indicating the absence of Emodin aggregates in the dispersions. Therefore, our results indicate that EMH is inserted into the lipid membrane, probably in the monomeric form at insertion depths, which do not allow contact with the water molecules.

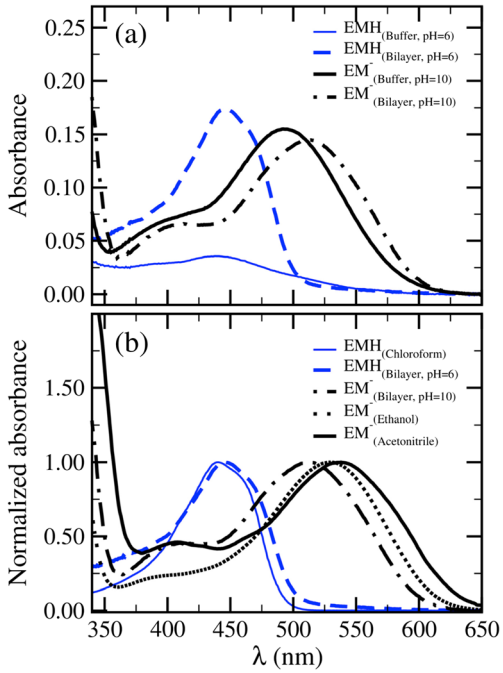

Fig. 3 (**a**) Optical absorption spectra of 0.02 mM neutral Emodin (EMH) at pH = 6.0 and anionic/deprotonated Emodin (EM^-) at pH = 10.0, in buffer solutions (*solid lines*) and in DMPC dispersions (*dashed lines*). (**b**) Normalized absorption spectra of EMH in DMPC dispersion and in chloroform (*blue solid line*) and of EM^- in DMPC dispersion and in ethanol (*black dotted line*) and in acetonitrile (*black solid line*)

Figure 3 (a) also shows the absorption spectra of EM^- in lipid dispersion and buffer solution, both at pH = 10. These spectra present an intense band centered at 514 nm (lipid dispersion) and 492 nm (buffer solution). Thus, the presence of EM^- in the DMPC bilayer shifted the band to higher wavelengths by 22 nm. Under high pH conditions, the UV-Vis absorption spectra of the Emodin are very sensitive to the environment. In alkaline solutions, the main absorption band is red-shifted by 11 nm with a solvent change water → ethanol, by 14 nm with water → 2-propanol, 19 nm with water → acetonitrile and 34 nm with water → DMSO, as previously discussed in the supplementary material of da Cunha et al. (2014). Therefore, the observed red shift of 22 nm in the bilayer is close to those found for changing water → acetonitrile and water → alcohols, indicating that the EM^- in lipid dispersions seems to be located in an environment that mimic the polarity of acetonitrile or alcohols (ethanol and 2-propanol), probably at the polar head group region of the lipid bilayer. This fact leads us to suggest that EM^- is located in the bilayer at a region that may favor strong effects on DMPC polar head groups.

As shown before (da Cunha et al. 2014), the absorption spectra of EMH is not dependent on the solvent polarity. Figure 3(b) compares the absorption spectra of EMH in DMPC dispersion and in chloroform. Although we have chosen chloroform, any other non-aqueous solvent provides the spectral signature of EMH in the solvent (Pal and Jana 1993; Nguyen et al. 2008; da Cunha et al. 2014). The similarity between the EMH spectra in DMPC dispersion and in organic solvents clearly indicates that EMH is inserted into the DMPC bilayer. For EM^-, Fig. 3(b) shows that either the spectrum obtained in acetonitrile or in ethanol provides good agreement with the spectrum of this species in DMPC dispersion, indicating that EM^- is located in the bilayer in an environment similar to these organic solvents, hence close to DMPC glycerol groups.

Theoretical results

In Table S1 (in Supplementary Material) are listed the values of the area per lipid (A_L), volume per lipid (V_L), the isothermal area compressibility modulus K_A, thickness of the bilayer (D_{HH}), hydrocarbon thickness (D_c) and Luzzati thicknesses (D_B) for the purpose of literature data that validated molecular simulations of DMPC bilayers (Poger and Mark 2010; Moore et al. 2001; Lopez et al. 2004; Zubrzycki et al. 2000; Gierula et al. 1999; Sachs et al. 2003; Jämbeck and Lyubartsev 2012). The A_L was calculated from the total lateral area of the simulation box divided by the number of lipids in each lipid monolayer. The time evolution of A_L is an indicator to evaluate the equilibrium of lipid bilayers, and its average value is often used in the validation of lipid force field parameters and their ability to reproduce experimental properties. Figures S1 and S2 (in Supplementary Material) shows the time evolution of area per lipid, A_L, volume per lipid, V_L, total energy, E_T, and potential energy, U_p, indicating that, for all the simulations, pure-DMPC, DMPC + EMH and DMPC + EM^-, the equilibrium was achieved before 50 ns. This ensures that the systems are at equilibrium when the data were calculated over the last 100 ns of the simulation with pure-DMPC and 150 ns for DMPC + EMH and DMPC + EM^-. For all the systems, the average values of A_L and V_L are 0.602 ± 0.005 nm^2 and 1.052 ± 0.003 nm^3, in excellent agreement with the experimental values (A_L in the range of 0.58–0.67 nm^2 (Davis et al. 2009; De Young and Dill 1988; Smaby et al. 1997; Lis et al. 1982; Rand and Parsegian 1989; Koenig et al. 1997; Petrache et al. 1998; Nagle and Tristram-Nagle 2000) and V_L with values of 1.09 and 1.10 nm^3 (Petrache et al. 1998; Nagle and Tristram-Nagle 2000; Sabín et al. 2009; Costigan et al. 2000)). Thus, adding Emodin in very small concentration (either EMH or EM^-) to the lipid bilayer does not affect the overall lipid organization. The values of E_T and U_p are $-2.353 \pm 0.005 \times 10^5$ kcal/mol and $-2.780 \pm 0.005 \times 10^5$ kcal/mol for DMPC + EMH and $-2.354 \pm 0.005 \times 10^5$ kcal/mol and $-2.781 \pm 0.005 \times 10^5$ kcal/mol for DMPC + EM^-. As expected, the fluctuation of the energy terms are must larger then the difference of the two systems due to the deprotanation of one Emodin molecule.

Considering that Emodin has both lipophilic and hydrophilic groups, its interaction with the lipid bilayer plays a significant role in understanding its biological activities. Thus, before detailing our results, we briefly focus on the stability of Emodin in gas phase and aqueous solution. As we have discussed before (da Cunha et al. 2014), both EMH and EM^- are stable in gas phase and aqueous solution with their dipole moments (μ) dependent on the environment: for EMH $\mu_g = 2.7$ D and $\mu_{aq} = 3.5$ D and for EM^- $\mu_g = 8.5$ D and $\mu_{aq} = 12.9$ D, where the solvent has described in the QM calculation with the PCM model and the origin of the Cartesian coordinates was considered as the center-of-charge distribution in the case of EM^-. As can be seen, there is an increase of approximately 30 and 50% of the dipole moment of the neutral and deprotonated forms of Emodin, respectively, in water compared to vacuum. Analyzing the atomic charges (see Table S2 in Supplementary Material) of the Emodin in vacuum (CS0) and in water (CS1), we identified an increase in the modules of the charges of CS1 compared to CS0. These increases were mostly observed in the three oxygen atoms of the hydroxyl groups (O1, O3 and O8) and in the two oxygen atoms of the carbonyl groups (O9 and O10). In the case of EMH, the oxygen atoms O1, O3 and O8 have almost the same charge (around −0.63 in vacuum and −0.68 in water, an increase of ~8%). However, the oxygen atoms O9 and O10 have distinct charges (−0.64 and −0.49 in vacuum and −0.67 and −0.57 in water, an increase of 5% in O9 and 16% in O10). In the case of EM^-, the three oxygen atoms of the hydroxyl groups have almost the same charge in vacuum (around −0.71), but became distinct in water, leaving the deprotonated oxygen more negative than the others (around −0.72 for O1 and O8 and −0.84 for O3). Therefore, the CS0 and CS1 charge sets present large differences in charge distributions, and this fact leads us to expect distinct location, interaction and structural proprieties of Emodin in the lipid bilayer. On the other hand, the CS0 charge set cannot produce an appropriate description of interaction of Emodin with the molecules of medium, because it does not distinguish the deprotonation sites. Thus, the solvent effect on the electronic polarization of Emodin is important and cannot be neglected for a good description of its interaction with the environment. For this reason, all our results will be discussed with Emodin described by the CS1 charge set, but we present in the Supplementary Material (see Fig. S3) the analysis of location and structural properties (electron density profile) of Emodin described by CS0 and CS1 charge sets in the lipid bilayer. The simulations showed that both EMH and EM^- have the ability to insert into the membrane even for those simulations that started from initial configurations with Emodin at the top of bilayer (see Fig. 2b). For these simulations, the species were able to insert into the bilayer in 10 ns (see Fig. S4 in Supplementary Material). The CS0 and CS1 charge sets produced almost the same location of species in the bilayer, close to the glycerol group of DMPC, but the Emodin described by the CS0 charge set is slightly more buried in the lipid bilayer compared to the CS1 charge set. Therefore, all our results will also be discussed with Emodin inserted in the lipid bilayer.

Location and orientation of Emodin in the lipid bilayer

Figure 4a, b presents the time evolution for the *z* coordinates of center of mass (CM) of Emodin, oxygen atom O3 and methyl carbon (C15) (see Fig. 1), all relative to the center of the bilayer. From these figures, it becomes evident that the Emodin is in equilibrium positions in the bilayer for the last 150 ns of the simulations. The trajectories of the center of mass of both species of Emodin were compared: for EMH $z_{CM} = 1.14 \pm 0.04$ nm and for EM^- $z_{CM} = 1.51 \pm 0.04$ nm. Thus, we found that the EMH is more deeply inserted in the bilayer than EM^- by 0.4 nm. In addition, comparing the average positions of O3 and C15 atoms: for EMH $z_{O3} = 1.43 \pm 0.04$ nm and $z_{C15} = 0.77 \pm 0.04$ nm and for EM^- $z_{O3} = 1.96 \pm 0.04$ nm and $z_{C15} = 1.11 \pm 0.04$ nm, we observed that the methyl carbon atom is closer to the center of the bilayer than O3, where the difference between the average positions of O3 and C15 atoms for EMH is $\Delta z = 0.66$ nm and for EM^- is $\Delta z = 0.85$ nm. As the aromatic rings between O3 and C15 are almost rigid, these Δz values are the intramolecular O3-C15 distance projected in the *z*-axis (normal axis of the bilayer). Therefore, comparing these values with that one obtained directly from the optimized geometry of Emodin, $\Delta z_{opt} = 0.98$ nm, it is easy to notice that the average orientation of Emodin in relation to the normal axis of the approximately 47° and 28° for EMH and EM^-, respectively. To better understand the orientation of Emodin in the bilayer, it was analyzed by the probability distribution function of the angle, P(θ), between the C15-O3 axis and bilayer normal axis (*z*). The P(θ) for the EMH and EM^- species are illustrated in Fig. 4c. Analyzing this figure, we identify that the Emodin species have distinct orientations in the bilayer. In the case of EMH, the probability distribution exhibits a broad peak centered at 45° and with maximum at 36°, revealing that this species assumes different orientations during the simulations within the range of 0–85°. In the case of EM^-, the P(θ) presents a narrower distribution with a range of 0–60° and a maximum at 16°. Comparing the P(θ) for the species, it is found that neither species in the bilayer is aligned with the *z*-axis, but assumes preferential orientation characteristics. The most dominant orientations of the species in the bilayer have been characterized for EMH as $0 = 45 \pm 20°$ and for EM^- as $\theta = 16 \pm 10°$, where the uncertainties were estimated as the half widths of the distributions.

To characterize in more detail the location of Emodin in the bilayer, we computed the electron density profile across the bilayer (see Fig. 5, and Fig. S5 in Supplementary Material) for the different system components and for the contributions from DMPC groups namely choline, phosphate, glycerol_1 and glycerol_2

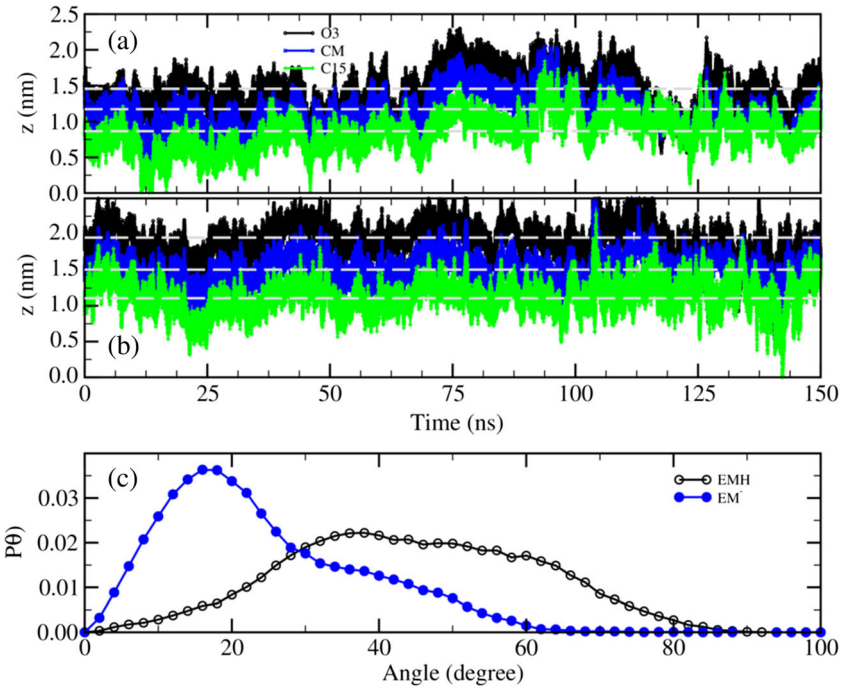

Fig. 4 Time evolutions for the z coordinates of the center of mass (*CM*) of the Emodin, oxygen atom O3 and methyl carbon (*C15*) for the EMH (**a**) and EM^- (**b**), all relative to the center of the bilayer. (**c**) Probability distribution function of the angle, P(θ), between the C15-O3 axis of the Emodin molecule and the bilayer normal axis (z) for the EMH (*open symbol*) and EM^- (*closed symbol*). *Dashed lines* in (**a**) and (**b**) represent the average z coordinates

(defined in Fig. S6 in Supplementary Material). Due to the low electron density of EMH and EM^-, their profiles were scaled by a factor of 50. The figures show that the EMH and EM^- are inside the lipid bilayer at positions close to the glycerol groups. However, the species EMH is slightly closer to the center of the bilayer. On close inspection, it can be seen that the electron density profiles of the EMH and EM^- are approximately a Gaussian distribution, where the maximum positions relative to the center of the bilayer are dislocated at 1.14 ± 0.20 and 1.52 ± 0.30 nm, respectively. The difference between these positions is 0.4 nm, therefore in complete agreement with the value obtained from Fig. 4a, b.

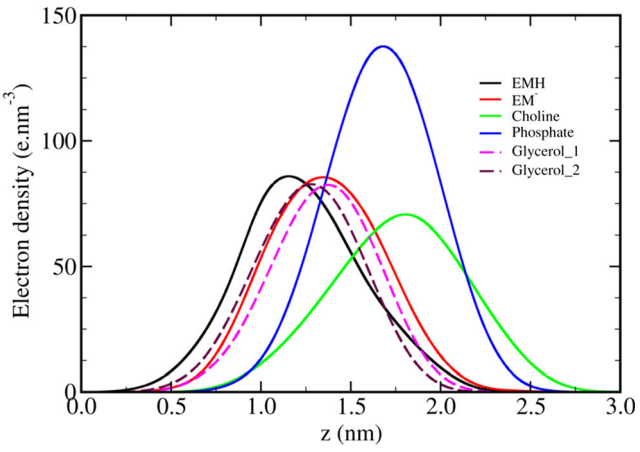

Fig. 5 Electron density profiles of the contributions stemming from components EMH, EM^-, choline, phosphate, glycerol_1 and glycerol_2. The electron density profiles of EMH and EM^- have been multiplied by 50

Structure and interactions of Emodin with water and lipid bilayer

Structural modifications of the Emodin, especially due to breaking its intramolecular hydrogen bonds by interaction with the environment, are considered to account for the diverse biological activities of this molecule. As discussed before (da Cunha et al. 2014), the geometries of the Emodin are planar presenting intramolecular hydrogen bonds (IHB) accepted by the carbonyl oxygen at C9. It is interesting to emphasize that the break of IHB of the Emodin involves a change in the dipole moment of the EMH and EM^- in the range of 1.8–4.9 D and 6.8–8.8 D in vacuum and of 2.9–6.6 D and 7.5–11.0 D in water (see Fig. S7 in Supplementary Material). Therefore, it is interesting to examine how the lipid bilayer affects the structure of the Emodin, and whether there are differences between these structures in aqueous solution and in the lipid bilayer. To investigate the structure of the species in these environments, we calculated the dihedral angle probability distribution function for the dihedral angles dh1 (C2-C1-O1-H1), dh3 (C2-C3-O3-H3) and dh8 (C7-C8-O8-H8), which are angles associated with O1H1, O3H3 and O8H8 hydroxyl groups, respectively (see dihedral in Fig. 1). The conformations of these angles were classified as *without_IHB* ($0° \leq \phi < 30°$ or $330° \leq \phi < 360°$), *transition_IHB* ($30° \leq \phi < 150°$ or $210° \leq \phi < 330°$) or *with_IHB* ($150° \leq \phi < 210°$).

Figure 6 shows the dihedral angle probability distribution for the dihedral dh1 (Fig. 6a) and dh3 (Fig. 6b) of the EMH species in water and the lipid bilayer. This figure reveals that the dihedral dh3 is highly flexible, changing conformations frequently during the simulations. However, in both environments, we observed that this dihedral is more often found in the

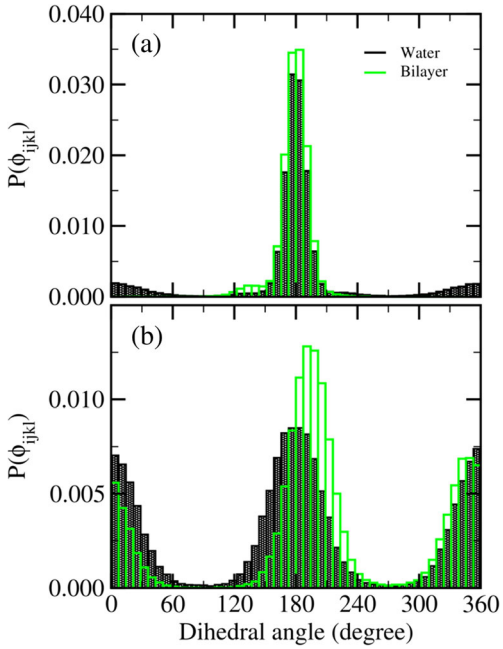

Fig. 6 (**a**) Probability distribution of the dihedral angles dh1 (C2-C1-O1-H1) and in (**b**) of the dh3 (C2-C3-O3-H3) of EMH in water (*solid bars*) and lipid bilayer (*open bars*) calculated from the simulations of water + EMH and DMPC + EMH. The angles dh1 and dh8 (C7-C8-O8-H8) have exhibit the same behavior during the simulations of EMH in both environments

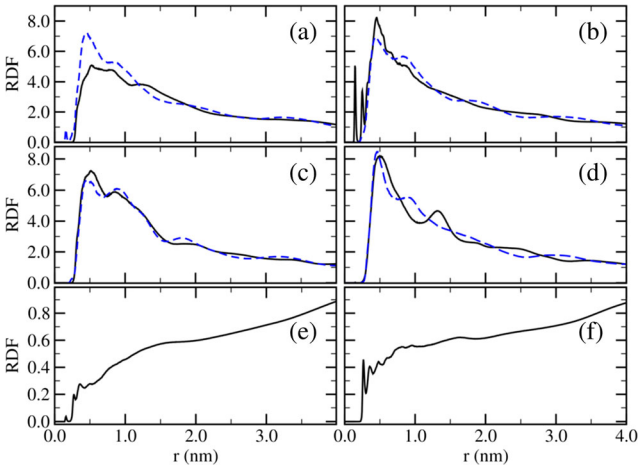

Fig. 7 Radial distribution function (*RDF*) between the Emodin and individual components of the DMPC molecule and Emodin and oxygen of water molecule (*Ow*): (**a**) EMH-choline (*solid line*) and EMH-phosphate (*dashed line*), (**b**) EMH-glycerol_1 (*solid line*) and EMH-glycerol_2 (*dashed line*), (**c**) EM$^-$-choline (*solid line*) and EM$^-$-phosphate (*dashed line*), (**d**) EM$^-$-glycerol_1 (*solid line*) and EM$^-$-glycerol_2 (*dashed line*), (**e**) EMH-Ow and (**f**) EM$^-$-Ow

conformation with ϕ in the range of 150–210° than in the other conformations. The angles dh1 and dh8 behave similarly during the simulations of EMH in aqueous solution and in the lipid bilayer. We observed these dihedrals as rigid, remaining almost the entire time of the simulation in the *with_IHB* conformation, which is the conformation in which the O1H1 and O8H8 hydroxyls are forming intramolecular hydrogen bonds (H1 and H8 with O9). Our simulations reveal, however, that breaking of intra-HB of EMH and EM$^-$ depends on the environment in which the molecule is immersed, since they break more often in pure water than in the lipid bilayer. For example, the O8H8 hydroxyl of both EMH and EM$^-$ in water remain at about 68 and 91%, respectively, and in the lipid bilayer these percentages are 94 and 99%, respectively, of the total simulation time.

We also performed thae study of the interaction of the Emodin in the bilayer in terms of radial distribution functions (RDFs) of lipids and water molecules around this molecule. Figure 7 shows the RDFs of the Emodin and head groups (choline, phosphate, glycerol_1 and glycerol_2) of the lipids and of the Emodin and oxygen of the water molecules. Figure 7a–d shows that the distribution of DMPC around the Emodin species are similar, but there are some noticeable differences in the RDFs of the lipid head groups. Comparing these functions, we notice more pronounced shapes of peaks for EM$^-$ than for EMH, indicating that the packing and distribution of DMPC around species are different. Two peaks centered at 0.5 and 1.3 nm, which correspond to the first and second lipid shells, are present in the distribution of the glycerol_1 around the EM$^-$. For EMH, we observe two peaks at 0.1 and 0.2 nm that are normally attributed to intermolecular hydrogen bonds (HB) and an additional peak at 0.5 nm that corresponds to the first lipid shell. Note that the RDFs of EM$^-$ do not exhibit these HB peaks, indicating that hydrogen bonds are not formed between EM$^-$ and the lipids. The RDF between the Emodin and the oxygen atom of water are shown in Fig. 7e (EMH) and 7f (EM$^-$). Two peaks are seen centered at 0.16 and 0.27 nm in the EMH-Ow curve and a peak centered at 0.26 nm in the EM$^-$-Ow curve, which are also due to hydrogen bonding between the Emodin and water molecules.

The intermolecular hydrogen bonds (HB) between the Emodin and environmental molecules are also analyzed using the geometric criteria, considering the distance between the acceptor (A) and donor (D) atoms involved in the HB (R_{D-A}) and the angle between the vector defined by the acceptor-donor atoms and the vector defined by the Hydrogen-donor bond ($\theta_{A\text{-}HD}$). We consider an HB formation when $R_{D-A} \leq 0.315$ nm and the angle $\theta_{A\text{-}HD} \leq 30°$ (Canuto and Coutinho 2000; Jorgensen et al. 1983). For the interaction between the Emodin and the lipid molecules, we find 1.00 and 0.01 hydrogen bonds for EMH and EM$^-$, respectively, revealing that the EM$^-$- lipid HBs are almost negligible. We have in addition analyzed the HB interactions between the EMH and DMPC groups (choline, phosphate, glycerol_1 and glycerol_2). The results show that the dominant interactions in this case are EMH-glycerol_1 and EMH-phosphate, which are responsible for 74 and 25% of all EMH-lipid hydrogen bonds, respectively. Our results also show that the interactions between the O3H3 hydroxyl and DMPC groups (phosphate and glycerol_1) are the strongest among the three

hydroxyl groups, followed by O1H1 and O8H8. For these hydroxyls, we registered 88% (O3H3), 8% (O1H1) and 4% (O8H8) of all the EMH–lipid hydrogen bonds. Thus, our simulations suggest a direct correlation of conformational changes of these hydroxyls with its HB interactions. The O3H3 hydroxyl, for instance, is the most flexible with the strongest HB interactions with both lipid and water molecules, as will be shown below, whereas the O8H8 hydroxyl is most rigid with the fewest HB-interactions with environment molecules.

We also examined, in both environments, the HB between the Emodin species and water molecules. In Table 1, we summarize the average number of HB between these groups and water molecules. The number of hydrogen bonds formed between the EMH and water molecules are 7.2 and 2.4 HB for this species in pure water and in the lipid bilayer, respectively. For EM^-, however, these numbers are 9.5 and 5.7 HB. These data reveal that the HB interaction of EM^- with water molecules are greater than of EMH. However, we observed a dehydration of both species in the lipid bilayer, but that for EMH is more noticeable.

A detailed analysis of interactions between hydroxyl and carbonyl groups of the Emodin and water molecules revealed that, in both environments, lipid bilayer and water, the interactions of O3H3(EMH) and O3(EM^-) with water molecules are larger among all the groups analyzed (see Table 1). The results show that the transfer of Emodin from pure water to a lipid bilayer reducesthe average number of HB by approximately 42, 93 and 59% for the hydroxyl groups O1H1, O8H3 and O3H3 of EMH and 47, 93 and 6% for these groups in the EM^-, respectively, (note that O3H3 becomes O3), revealing a strong dehydration of these groups in both species, but for EM^- this effect is less pronounced. For both EMH and EM^-, we observe that the dehydration of O8H8 represents double that of O1H1. This occurs mainly due to the position and orientation of these hydroxyls in the lipid bilayer, maintaining the O8H8 that is more distant from bulk water than O1H1.

It is interesting to note that the weak HB -interactions of the O1H1 and O8H8 hydroxyls with water in both environments is mainly due to the two intra-HBs formed between these hydroxyls and the C9O9 carbonyl, which reduces the interaction of the carbonyl group with water. These intra-HBs play an important role in the hydrophilic/lipophilic character of Emodin species that can be seen in the large difference between the number of inter-HB of this carbonyl group in pure water and in the lipid bilayer. There is a decrease of about 90% of inter-HB number formed between the C9O9 and water molecules for both species in the lipid bilayer. This feature, together with strong intra-HB of both EMH and EM^- in the lipid bilayer, increases the lipophilic character of the Emodin and favors its stability in this amphiphilic environment.

Table 1 Statistics of the hydrogen bonds formed between the hydroxyl and carbonyl groups of the Emodin species and water in the lipid bilayer and in pure water

Group	Lipid bilayer		Water	
	EMH	EM^-	EMH	EM^-
O1H1	0.7	0.8	1.2	1.5
O8H8	0.1	0.1	1.4	1.5
O3H3/O3	0.9	3.3	2.2	3.5
O9	0.1	0.1	0.8	1.1
O10	0.6	1.4	1.6	1.9
Total	2.4	5.7	7.2	9.5

Effect of Emodin on the lipid bilayer

We also examined the structural properties of the lipid bilayer in the vicinity of Emodin and quantified the effect of each Emodin specie in these properties. We defined this region considering the number of lipid and water molecules within a shell of radius of 1 nm around the species. This choice of 1 nm was motivated by the RDF of glycerol_1 and the electron density results discussed above. These molecules were accounted considering the shortest distance between all the atoms in the molecules (lipid or water) and the center of mass of the EMH and EM^- species. Figure 8a shows the probability distributions of the number of lipids around both EMH and EM^-. This figure shows that there are almost the same number of lipids around the species, about 5 for EMH and 4 for EM^-.

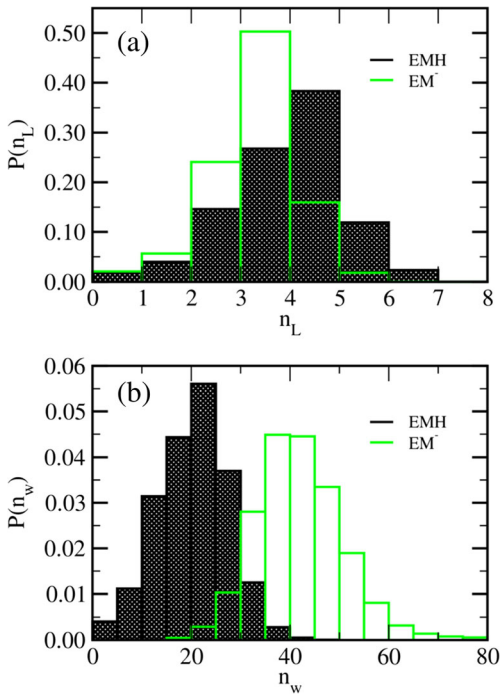

Fig. 8 Probability distribution of the number of lipid (**a**) and water (**b**) molecules around the Emodin (EMH *solid bars* and EM^- *open bars*) within a shell of radius 1 nm, calculated from simulations of DMPC + EMH and DMPC + EM^-

Furthermore, this figure indicates asymmetric distributions with probabilities of finding 4 and 6 lipids around the EMH of 27 and 12%, respectively. For EM^-, the probabilities of finding 3 and 5 lipids are 25 and 16%, respectively. These findings show small differences between the arrangement of lipid molecules around the EMH and EM^-, leading to different values of area per lipid in the vicinity of the species. We observe an increase in the area per lipid of ~4% for EMH and ~30% for EM^-, from 0.602 ± 0.005 nm^2 in pure-DMPC to 0.628 ± 0.005 and 0.785 ± 0.005 nm^2 in the presence of EMH and EM^-, respectively. Figure 8b shows the probability distributions for the number of water around of EMH and EM^-. The analysis of this figure provides about 21 and 43 water molecules around the EMH and EM^- species, respectively, giving the same information obtained in the analysis of hydrogen bonds discussed above that the hydration of EM^- is more than twice that of EMH. Therefore, our simulations show that the number of water molecules present in the lipid bilayer regions to interact with EM^- is substantially larger than the corresponding number for EMH.

Additionally, we calculated the deuterium order parameters S_{CD} profiles (Brown 1996) of acyl chains of lipids within the vicinity of Emodin and compared them with the profiles calculated from the simulations of pure-DMPC. Figure 9 shows the $|S_{CD}|$ profiles of the lipid sn-1 (Fig. 9a) and sn-2 (Fig. 9b) acyl chains calculated from the simulations of pure-DMPC, DMPC + EMH and DMPC + EM^-, considering only the lipids within the vicinity of Emodin. In all three cases, the $|S_{CD}|$ profiles exhibit values lower than 0.23, indicating a greater disorder of the hydrocarbon chains. In the case of pure-DMPC, our simulations reproduced the experimental (Petrache et al. 2000; Vermeer et al. 2007; Douliez et al. 1995) and theoretical (Poger and Mark 2010; Jämbeck and Lyubartsev 2012) $|S_{CD}|$ values of the sn-1 and sn-2 reported previously, with $|S_{CD}|$ profiles presenting an increase in the $|S_{CD}|$ values over the first five carbons of sn-1 and a plateau in the values of the correspondent atoms in the sn-2, followed by a decrease in magnitude of these parameters for the last six carbons of both the sn-1 and sn-2 acyl chains.

In the case of DMPC + EMH and DMPC + EM^-, we observe a larger effect on the order parameters of the sn-1 and sn-2 acyl chains of lipids in the Emodin vicinity compared to pure-DMPC simulations. The $|S_{CD}|$ profiles for the system with Emodin show an increase in the order parameters of the first two carbons of sn-1 hydrocarbon chains and a disruption of the plateau region of the order parameter at the initial part of the sn-2 chains, followed by a noticeable decrease at the last nine carbons of both sn-1 and sn-2 acyl chains, compared to pure-DMPC simulations. Thus, for these carbons, the sn-1 and sn-2 acyl chains of lipids around both EMH and EM^- are clearly less ordered than the correspondent chains in the pure-DMPC. However, for these carbons, the simulation with EMH yielded $|S_{CD}|$ values 0.01–0.04 lower than the simulations with EM^-, indicating that the effect of EMH on the order parameters is substantially larger than that of EM^-.

Although the effect on acyl chains of the EMH species is more pronounced than EM^-, this perturbing seems not to be stronger on structural properties of the lipid bilayer than the effect on the head groups caused by EM^-. This becomes more evident in the comparison of the electron density profiles across the lipid bilayers for the contributions from 5 lipid molecules of the pure-DMPC bilayer and from 5 lipid

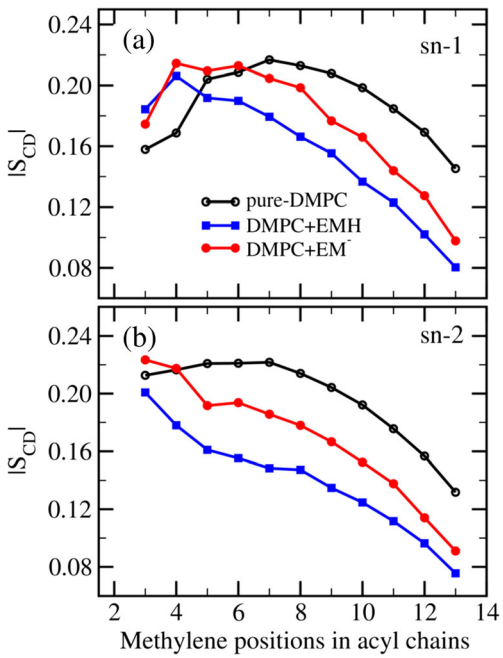

Fig. 9 Deuterium order parameter $|S_{CD}|$ profiles of the sn-1 (**a**) and sn-2 (**b**) fatty acyl chains of DMPC calculated from the simulations of pure-DMPC (*open symbols*), DMPC + EMH (*closed squares*) and DMPC + EM^- (*closed circles*), where were taken into account only five DMPC molecules in the vicinity of the Emodin species in the hydrated bilayer

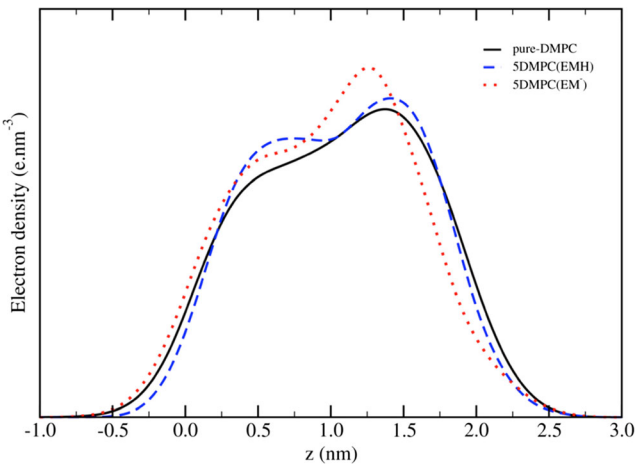

Fig. 10 Electron density profiles of the hydrated DMPC bilayer and of the contributions stemming from 5 DMPC molecules from the vicinity of the Emodin species calculated from the simulations of pure-DMPC, DMPC + EMH and DMPC + EM^-

Table 2 Summary of some results obtained with MD simulations for molecules of biological interest, which have hydrophilic and hydrophobic groups, interacting with phospholipid bilayers

Molecule Names	Lipid	Location	Force Field	Reference
Cholesterol	DPPC and DMPC	Inside	Berger, AMBER	Robinson et al. 1995; Gabdouline et al. 1996; Smondyrev and Berkowitz 1999; Hofsäß 2003.
Cholesterol, Ergosterol and Lanosterol	DMPC	Inside	AMBER	Smondyrev and Berkowitz 2001.
Fusidic acid	DPPC	Inside: at the head–tail interface	Berger	Falck et al. 2006.
Lidocaine (uncharged)	DMPC	Inside: at the head–tail interface, near the ester groups	Berger	Högberg et al. 2007.
Lidocaine (charged)	DMPC	Inside: at the headgroup region	Berger	Högberg et al. 2007.
Catechins	POPC	Inside: at the headgroup region	OPLS	Sirk et al. 2009.
Ibuprofen (uncharged)	DMPC	Inside: at the headgroup region	CG, Berger	Boggara and Krishnamoort 2010; Loverde 2014.
Ibuprofen (uncharged)	DPPC	Inside: at the acyl tails region	CG, Berger	Boggara and Krishnamoort 2010; Loverde 2014.
Ibuprofen (charged)	DPPC	Inside: at the headgroup region	Berger	Boggara and Krishnamoort 2010.
Aspirin (uncharged)	DPPC	Inside: at the acyl tails region	Berger	Boggara and Krishnamoort 2010.
Aspirin (charged)	DPPC	Inside: at the headgroup region	Berger	Boggara and Krishnamoort 2010.
Limonene, Perillyl alcohol, Perillaldehyde, and Perillic acid	DMPC and POPC	Inside: partitioned in the bilayer	Berger	Witzke et al. 2010.
Alprenolol, atenolol, pindolol, progesterone, testosterone	DMPC	Inside: at the headgroup region	CG, GAFF	Orsi and Essex 2010.
Stilbenoid	DPPC	Inside: at the headgroup region	GROMOS	Koukoulitsa et al. 2011.
Prodan	DLPC	Inside: depends on the atomic set of charges including different environment polarization	Berger	Nitschke et al. 2012.
Diploptene and Bacteriohopanetetrol	POPC	Inside: partitioned in the bilayer	GROMOS 53A6	Poger and Mark 2013.
Curcumin	DPPC and DMPG	Inside: at the headgroup region	OPLS	Jalili and Saeedi 2016.
Emodin (uncharged)	DMPC	Inside: at the head–tail interface, near the glycerol group	GROMOS 54a7	This work.
Emodin (charged)	DMPC	Inside: at the head–tail interface, near the glycerol group	GROMOS 54a7	This work.

molecules around the Emodin in the hydrated bilayers (see Fig. 10). Comparing these profiles, we found that both species induce modifications in the bilayer; however, different for each species. The EMH profile is very similar to the pure-DMPC profile, in the head group region of the lipid bilayer, whereas there is a noticeable difference in the hydrophobic region. Interestingly, in the case of EM^-, the electron density profiles present similarity in the acyl chains regions and large modifications in the head group region of the lipid bilayer. Furthermore, when compared with the pure-DMPC and DMPC + EMH profiles, the main peak in the density profile due to the phosphorus atoms in the vicinity of EM^- is shifted by 0.4 nm toward the center of the bilayer. Thus, the EMH causes greater disorder in the acyl chains region, but the EM^- causes greater perturbation in the head group region, bringing the phosphate group for a deeper position (~0.4 nm) caused by a larger amount of water molecules that penetrates the bilayer up to the glycerol region due to its interactions with the deprotonated oxygen of Emodin. Therefore, although both species of Emodin, EMH and EM^-, locate inside the bilayer in the same region, near the glycerol group the EM^- causes larger perturbations in the lipid bilayers.

Conclusions

In this work, we have investigated the effect of Emodin on the lipid bilayer of DMPC using experimental and theoretical techniques. We analyzed the halochromic and solvatochromic effects on absorption UV-Vis spectra of the neutral form (EMH) and the anionic/deprotonated form (EM^-) of Emodin compared with the spectra in the lipid bilayer, and we identified that the Emodin is inserted into the DMPC bilayer with the EM^- at regions with polarity similar to acetonitrile/ethanol, i.e., near the glycerol group. Our results are in agreement with the experimental results obtained previously (Alves et al.

2004), which indicated that the EMH is located at the upper part of the phospholipid acyl chains in the lipid bilayer. To our knowledge, no experimental studies have been performed for EM^- in a lipid bilayer. Interestingly, our results revealed that this anionic species is also located in the lipid bilayer. However, it is well known (Alberts et al. 2002; Sirka 2014, that lipid bilayers are highly impermeable for charged molecules and their hydration shell.

Using molecular dynamics simulations, we obtained detailed information of the localization of both EMH and EM^- in a fully hydrated DMPC lipid bilayer in the fluid phase. We observed that both EMH and EM^- described by the vacuum and aqueous solution charge distributions are buried in the lipid bilayer, specifically close to the glycerol groups of the lipids. These results are in good agreement with our experimental results discussed here, whereas they indicated that both species are located into the lipid bilayer with the EM^- at regions with polarity similar to ethanol/acetonitrile. We have compared the location and orientation of EMH and EM^- in the bilayer by monitoring various structural properties. We found that both species have similar locations in the bilayer. However, the EMH is inserted more deeply (~0.4 nm) into the bilayer. Considering the orientation, the EMH is more bent than EM^- compared with the normal z-axis of the bilayer, $\theta = 45 \pm 20°$ and $16 \pm 10°$, respectively, causing later perturbations in the acyl chains orientations. We have also compared the structural properties of Emodin in the lipid bilayer and in pure aqueous solution. We observed that both EMH and EM^- are more rigid (considering the rotation of the hydroxyl groups) in the bilayer than in aqueous solution. Then, in the amphiphilic environment, the intramolecular hydrogen bonds became stronger and this structural characteristic decreases the dipole moment of the Emodin, causing an increase in its lipophilic character and favoring its stability in lipid environments.

We have also revealed the hydrogen bonding interactions of both EMH and EM^- with lipid and water molecules in the lipid bilayer and in the aqueous solution. We found nearly 1 and 0 lipid molecules forming hydrogen bonds with the EMH and EM^- in the bilayer, respectively. In the case of water, we found nearly 7 and 9 water molecules bonded to the EMH and EM^- in pure water, while in the bilayer, these numbers were 2 and 6 water molecules bonded to the Emodin species, respectively. Therefore, our results revealed a dehydration of Emodin in the bilayer when compared with pure water. However, this dehydration is significantly stronger for the EMH (~70%) than for the EM^- (~30%). The effect of Emodin species on the bilayer was also analyzed with respect to a hydrated pure-DMPC bilayer. Considering only the nearest five lipid molecules around the species in the hydrated bilayers DMPC + EMH and DMPC + EM^-, we obtained that both, EMH and EM^-, affect the lipid bilayer in the vicinity of Emodin, and are responsible for changes in structural properties such as the order parameters $|S_{CD}|$ profiles of the acyl chains of the lipids and the electron density profiles, both properties obtained of the five lipids around the species. The EMH affects the lipids bilayer more in the nonpolar region, whereas EM^- induces more perturbations in the head group region. Thus, the neutral EMH causes greater disorder in the acyl chains region, but the anionic EM^- causes greater perturbation in the head group region bringing the phosphate group for a deeper position (~0.4 nm), caused by a larger amount of water molecules (~6 H_2O) that penetrate the bilayer up to the glycerol region due to their interactions with the deprotonated oxygen of Emodin. Therefore, although both species of Emodin, EMH and EM^-, locate inside the bilayer in the same region, near the glycerol group, the lipid bilayer is more affected by the EM^- compared with the EMH. These disorders caused by Emodin should cause distinct effects on lipid bilayer including the disruptive effects that have been previously reported in some phospholipid bilayer (Alves et al. 2004; Huang et al. 2006). Further, the diversity of biological activities attributed to Emodin, such as antibacterial, anti-inflammatory, antiviral and anticancer cell migration and invasion may be also related to its disruptive effect on biological membranes.

To give a wider perspective of the results obtained with MD simulations for molecules of biological interest, which have hydrophilic and hydrophobic groups interacting with phospholipid bilayers, we now compare our results with some results previously obtained by other authors. We select papers that studied molecules that have some chemical groups similar to Emodin, such as aromatic and alkyl rings (hydrophobic groups) and hydroxyl and carbonyl groups (hydrophilic groups). A summary is presented in Table 2. It can be seen that all the simulations identify the location of the molecule inside the bilayer regardless of the force field and lipid type. In some cases, more than one location was found to be stable, as for instance Limonene, Perillyl alcohol, Perillaldehyde, Perillic acid (Witzke et al. 2010), and Diploptene and Bacteriohopanetetrol (Poger and Mark 2013), which are partitioned in the bilayer changing from one location to another. Other molecules, like Fusidic acid (Falck et al. 2006), uncharged Lidocain (Högberg et al. 2007) and Emodin (this work), prefer the head–tail interface near the ester or glycerol groups of the lipid. For those molecules that were studied in the neutral form (uncharged) and deprotonated form (charged), in general the uncharged form are located deeper in the bilayer, as expected.

In this work, we have emphasized that as important as the identification of the location of the molecule in the lipid bilayer is to understand the roles of the hydrophilic groups of the molecules. We have identified two major effects: one is the hydrophobic character of the molecule which can increase or decrease depending on the relative orientation of the hydroxyl groups in the amphiphilic environment that modify its dipole moment and, consequently, its interaction with the lipid and the water molecules; and the other is the amount of water that penetrates in the bilayer together with the molecules and

causes great distortion of the head groups distribution in the vicinity of the molecule that can induces disruption of the bilayer in a larger concentration.

Acknowledgements This work was partially supported by CNPq, CAPES, FAPESP, INCT-FCx, NAP-FCx(USP) and BioMol (Brazil). Additionally, ARC acknowledges the fellowship from CNPq/CAPES, and HS, MTL and KC research fellowships from CNPq.

Compliance with ethical standards

Conflict of interest Antonio R. da Cunha declares that he has no conflicts of interest. Evandro L. Duarte declares that he has no conflicts of interest. Hubert Stassen declares that he has no conflicts of interest. M. Teresa Lamy declares that she has no conflicts of interest. Kaline Coutinho declares that she has no conflicts of interest.

Ethical approval This article does not contain any studies with human participants or animals performed by any of the authors.

References

Alberts B, Johnson A, Lewis J, Raff M, Roberts K, Walter P (2002) Molecular biology of the cell, 4th edn. Garland, New York

Almeida JG, Preto AJ, Koukos PI, Bonvin AMJJ, Moreira IS (2017) Membrane proteins structures: a review on computational modeling tools. Biochim Biophys Acta 1859:2021–2039

Alves DS, Pérez-Fons L, Estepa A, Micol V (2004) Membrane-related effects underlying the biological activity of the anthraquinones emodin and barbaloin. Biochem Pharmacol 68:549–561

Anke H, Kolthum I, Laaatsch H (1980) Metabolic products of microorganisms. 192. The anthraquinones of the Aspergillus glaucus group. II. Biological activity. Arch Microbiol 126:231–236

Apostolova E, Krumova S, Tuparev N, Molina MT, Filipova T, Petkanchin I, Taneva SG (2003) Interaction of biological membranes with substituted 1,4-anthraquinones. Colloids Surf B 29:1–12

Barnard DL, Huffman JH, Morris JL, Wood SG, Hughes BG, Sidwell RW (1992) Evaluation of the antiviral activity of anthraquinones, anthrones and anthraquinone derivatives against human cytomegalovirus. Antivir Res 17:63–77

Becke AD (1993) Density-functional thermochemistry. III The role of exact exchange. J Chem Phys 98:5648–5652

Bemporad D, Essex JW, Luttmann C (2004) Permeation of small molecules through a lipid Bilayer: a computer simulation study. J Phys Chem B 108:4875–4884

Berendsen HJC, Postma JPM, van Gunsteren WF, DiNola A, Haak JR (1984) Molecular dynamics with coupling to an external bath. J Chem Phys 81:3684–3690

Berendsen HJC, Postma JPM, van Gunsteren WF, Hermans J (1981) Interaction models for water in relation to protein hydration. In: Pullman, B (ed) Intermolecular forces. Reidel, Dordrecht

Bi S, Zhang H, Qiao C, Sun Y, Liu C (2008) Studies of interaction of emodin and DNA in the presence of ethidium bromide by spectroscopic method. Spectrochim Acta Part A 69:123–129

Boggara MB, Krishnamoorti B (2010) Partitioning of nonsteroidal Antiinflammatory drugs in lipid membranes: a molecular dynamics simulation study. Biophys J 98:586–595

Breneman CM, Wiberg KB (1990) Determining atom-centered monopoles from molecular electrostatic potentials. The need for high sampling density in formamide conformational analysis. J Comp Chem 11:361–373

Brown MF (1996) Membrane structure and dynamics studied with NMR spectroscopy. In: Merz K, Roux B (eds) Biological membranes. Birkhäuser, Boston

Canuto S, Coutinho K (2000) From hydrogen bond to bulk: Solvation analysis of the n-π^* transition of formaldehyde in water. Int J Quantum Chem 77:192–198

Chan TC, Chang CJ, Koonchanok NM, Geahlen RL (1993) Selective inhibition of the growth of ras-transformed human bronchial epithelial cells by emodin, a protein-tyrosine inhibitor. Biochem Biophys Res Commun 193:1152–1158

Chen YC, Shen SC, Lee WR, Hsu FL, Lin HY, Ko CH, Tseng SW (2002) Emodin induces apoptosis in human promyeloleukemic HL-60 cells accompanied by activation of caspase 3 cascade but independent of reactive oxygen species production. Biochem Pharmacol 64:1713–1724

Choi RJ, Ngoc TM, Bae K, Cho HJ, Kim DD, Chun J, Khan S, Kim YS (2013) Anti-inflammatory properties of anthraquinones and their relationship with the regulation of P-glycoprotein function and expression. Eur J Pharmacol Sci 48:272–281

Costigan SC, Booth PJ, Templer RH (2000) Estimations of lipid bilayer geometry in fluid lamellar phases. Biochim Biophys Acta 1468:41–54

Cuendet MA, van Gunsteren WF (2007) On the calculation of velocity-dependent properties in molecular dynamics simulations using the leapfrog integration algorithm. J Chem Phys 127:184102–184110

da Cunha AR, Duarte EL, Lamy MT, Coutinho K (2014) Protonation/deprotonation process of Emodin in aqueous solution and pKa determination: UV/visible spectrophotometric titration and quantum/molecular mechanics calculations. Chem Phys 440:69–79

Davis JE, Rahaman O, Patel S (2009) Molecular dynamics simulations of a DMPC Bilayer using nonadditive interaction models. Biophys J 96:385–402

De Young LR, Dill KA (1988) Solute partitioning into lipid bilayer membranes. Biochemist 27:5281–5289

Ditchfield R, Hehre WJ, Pople JA (1971) Self-consistent molecular-orbital methods. IX An Extended Gaussian Type Basis for Molecular Orbital Studies of Organic Molecules. J Chem Phys 54:724–728

Dong X, Fu J, Yin X, Cao S, Li X, Lin L, Huyiligegi NJ (2016) Emodin: a review of its pharmacology, Toxicity and Pharmacokinetics. Phytother Res 30:1207–1218

Douliez JP, Léonard A, Dufoure EJ (1995) Restatement of order parameters in biomembranes: calculation of C-C bond order parameters from C-D quadrupolar splittings. Biophys J 68:1727–1739

Duarte EL, Oliveira TR, Alves DS, Micol V, Lamy MT (2008) On the interaction of the Anthraquinone Barbaloin with negatively charged DMPG Bilayers. Langmuir 24:4041–4049

Essmann U, Perera L, Berkowitz ML, Darden T, Lee H, Pedersen LG (1995) A smooth particle mesh Ewald method. J Chem Phys 103:8577–8593

Fabriciova G, Cortés SS, Ramos JVG, Miskovsky P (2004) Surface-enhanced Raman spectroscopy study of the interaction of the Antitumoral drug Emodin with human serum albumin. Biopolymers 74:125–130

Falck E, Hautala JT, Karttunen M, Kinnunen PKJ, Patra M, Saaren-Seppälä H, Vattulainen I, Wiedmer SK, Holopainen JM (2006) Interaction of Fusidic acid with lipid membranes: implications to the mechanism of antibiotic activity. Biophys J 91:1787–1799

Francke B, Moss H, Timbury MC, Hay J (1978) Alkaline DNase activity in cells infected with a temperature-sensitive mutant of herpes simplex virus type 2. J Virol 26:209–213

Frisch MJ et al (2004) Gaussian 03. Gaussian, Wallingford, CT

Fuchs J, Milbradt R, Zimmer G (1990) Multifunctional analysis of the interaction of anthralin and its metabolites anthraquinone and anthralin dimer with the inner mitochondrial membrane. Arch Dermatol Res 282:47–55

Gabdouline RR, Vanderkooi G, Zheng C (1996) Comparison of structures of dimyrstoylphosphatidylcholine in the presence and absence

of cholesterol by molecular dynamics simulation. J Phys Chem 96: 15942–15946
Ghomi M (2012) Applications of Raman spectroscopy to biology, vol 5. IOS, Amsterdam
Gierula MP, Takaoka Y, Miyagawa H, Kitamura K, Kusumi A (1999) Charge pairing of headgroups in phosphatidylcholine membranes: a molecular dynamics simulation study. Biophys J 73:1228–1240
Goldstein EB, Evron Z, Frenkel M, Cohen K, Meiron KN, Peer D, Roichman Y, Flescher E, Fridman M (2011) Targeting Anthracycline-resistant tumor cells with synthetic aloe-Emodin glycosides. ACS Med Chem Lett 2:528–531
Heimburg T (2007) Thermal biophysics of membranes. Wiley-VCH, Weinheim
Hernandez M, Recio G, Palma RJM, Ramos JVG, Domingo C, Sevilla P (2012) Surface enhanced fluorescence of anti-tumoral drug emodin adsorbed on silver nanoparticles and loaded on porous silicon. Nanoscale Res Lett 7:364–371
Hess B, Bekker H, Berendsen HJC, Fraaije JGEM (1997) LINCS: a linear constraint solver for molecular simulations. J Comput Chem 18: 1463–1472
Hofsäß C, Lindahl E, Edholm O (2003) Molecular dynamics simulations of Phospholipid Bilayers with cholesterol. Biophys J 84:2192–2206
Högberg CJ, Maliniak A, Lyubartsev AP (2007) Dynamical and structural properties of charged and uncharged lidocaine in a lipid bilayer. Biophys Chem 125:416–424
Hsiang CY, Ho TY (2008) Emodin is a novel alkaline nuclease inhibitor that suppresses herpes simplex virus type 1 yields in cell cultures. Br J Pharmacol 155:227–235
Huang HC, Chu SH, Chao PD (1991) Vasorelaxants from Chinese herbs, emodin and scoparone, possess immunosuppressive properties. Eur J Pharmacol 198:211–213
Huang Q, Shen HM, Ong CN (2004) Inhibitory effect of emodin on tumor invasion through suppression of activator protein-1 and nuclear factor-kappaB. Biochem Pharmacol 68:361–371
Huang Q, Shen HM, Ong CN (2005) Emodin inhibits tumor cell migration through suppression of the phosphatidylinositol 3-kinase-Cdc42/Rac1 pathway. Cell Mol Life Sci 62:1167–1175
Huang Q, Shen HM, Shui G (2006) Emodin inhibits tumor cell adhesion through disruption of the membrane lipid raft-associated Integrin signaling pathway. Cancer Res 66:5807–5815
Huang W, Lin Z, van Gunsteren WF (2011) Validation of the GROMOS 54A7 force field with respect to beta-peptide folding. J Chem Theory Comput 7:1237–1243
Imamura Y, Otsuka T, Nakai H (2007) Description of Core excitations by time-dependent density functional theory with local density approximation, generalized gradient approximation, meta-generalized gradient approximation, and hybrid Hunctionals. J Comput Chem 28: 2067–2074
Izhaki I (2002) Emodin – a secondary metabolite with multiple ecological functions in higher plants. New Phytol 155:205–217
Jalili S, Saeedi M (2016) Study of curcumin behavior in two different lipid bilayer models of liposomal curcumin using molecular dynamics simulation. J Biomol Struct Dyn 34:327–340
Jämbeck JPM, Lyubartsev AP (2012) Derivation and systematic validation of a refined all-atom force field for Phosphatidylcholine lipids. J Phys Chem B 116:3164–3179
Jayasuriya H, Koonchanok NM, Geahlen RL, McLaughlin L, Chang CJ (1992) Emodin, a protein tyrosine kinase inhibitor from Polygonum Cuspidatum. J Nat Prod 55:696–698
Jendrossek V, Handrick R (2003) Membrane targeted anticancer drugs: potent inducers of apoptosis and putative Radiosensitisers. Curr Med Chem Anticancer Agents 3:343–353
Jorgensen WL, Chandrasekhar J, Madura JD, Impey RW, Klein ML (1983) Comparison of simple potential functions for simulating liquid water. J Chem Phys 79:926–935
Kawai K, Kato T, Mori H, Kitamura J, Nozawa Y (1984) A comparative study on cytotoxicities and biochemical properties ofanthraquinone mycotoxinsemodin and skyrin from Penicillium islandicum. Toxicol Lett 20:155–160
Koenig BW, Strey HH, Gawrisch K (1997) Membrane lateral compressibility determined by NMR and x-ray diffraction: effect of acyl chain polyunsaturation. Biophys J 73:1954–1966
Koukoulitsa C, Durdagi S, Siapi E, Villalonga-Barber C, Alexi X, Steele BR, Micha-Screttas M, Alexis MN (2011) Comparison of thermal effects of stilbenoid analogs in lipid bilayers using differential scanning calorimetry and molecular dynamics: correlation of thermal effects and topographical position with antioxidant activity. Eur Biophys J 40:865–875
Koyama M, Kelly TR, Watanabe KA (1988) Novel type of potential anticancer agents derived from chrysophanol and emodin. Some structure-activity relationship studies. J Med Chem 31:283–284
Kumar A, Dhawan S, Aggarwal BB (1998) Emodin (3-methyl-1,6,8-trihydroxyanthraquinone) inhibits TNF-induced NF-B activation, IB degradation, and expression of cell surface adhesion proteins in human vascular endothelial cells. Oncogene 17:913–918
Kuo YC, Meng HC, Tsai WJ (2001) Regulation of cell proliferation, inflammatory cytokine production and calcium mobilization in primary human T lymphocytes by emodin from Polygonum Hypoleucum Ohwi. Inflamm Res 50:073–082
Lis LJ, McAlister M, Fuller N, Rand RP, Parsegian VA (1982) Interactions between neutral phospholipid bilayer membranes. Biophys J 37:657–665
Lopez CF, Nielsen SO, Klein ML, Moore PB (2004) Hydrogen bonding structure and dynamics of water at the Dimyristoylphosphatidylcholine lipid Bilayer surface from a molecular dynamics simulation. J Phys Chem B 108:6603–6610
Loverde SM (2014) Molecular simulation of the transport of drugs across model membranes. J Phys Chem Lett 5:1659–1665
Lucio M, Nunes C, Gaspar D, Ferreira H, Lima JLFC, Reis S (2009) Antioxidant activity of vitamin E and Trolox: understanding of the factors that govern lipid peroxidation studies in vitro. Food Biophys 4:312–320
MacCallum JL, Tieleman DP (2006) Computer simulation of the distribution of hexane in a lipid Bilayer: spatially resolved free energy, entropy, and enthalpy profiles. J Am Chem Soc 128:125–130
Malde AK, Zuo L, Breeze M, Stroet M, Poger D, Nair PC, Oostenbrink C, Mark AE (2011) An automated force field topology builder (ATB) and repository: version 1.0. J Chem Theory Comput 7: 4026–4037
Marković ZS, Manojlović NT (2009) DFT study on the reactivity of OH groups in emodin: structural and electronic features of emodin radicals. Monatsh Chem 140:1311–1318
Marsh D (1990) CRC handbook of lipid Bilayers. CRC, Boca Raton
Miertus S, Scrocco E, Tomasi J (1981) Electrostatic interaction of a solute with a continuum. A direct utilizaion of AB initio molecular potentials for the prevision of solvent effects. Chem Phys 55:117–129
Miyamoto S, Kollman PA (1992) An analytical version of the SHAKE and RATTLE algorithm for rigid water models. J Comput Chem 13: 952–962
Moore PB, Lopez CF, Klein ML (2001) Dynamical properties of a hydrated lipid Bilayer from a multinanosecond molecular dynamics simulation. Biophys J 81:2484–2494
Nagle JF, Tristram-Nagle S (2000) Structure of lipid bilayers. Biochim Biophys Acta 1469:159–195
Nguyen SC, Hansen BKV, Hoffmann SV, Spanget-Larsen J (2008) Electronic states of emodin and its conjugate base. Synchrotron linear dichroism spectroscopy and quantum chemical calculations. Chem Phys 352:67–174
Nitschke WK, Suplicy CCV, Coutinho K, Stassen H (2012) Molecular dynamics investigations of PRODAN in a DLPC Bilayer. J Phys Chem B 116:2713–2721

Nunes C, Brezesinski G, Lopes D, Lima JLFC, Reis S, Lúcio M (2011) Lipid–drug interaction: biophysical effects of Tolmetin on membrane mimetic Systems of Different Dimensionality. J Phys Chem B 115:12615–12623

Omote H, Al-Shawi MK (2006) Interaction of transported drugs with the lipid Bilayer and P-glycoprotein through a Solvation exchange mechanism. Biophys J 90:4046–4059

Orsi M, Essex JW (2010) Permeability of drugs and hormones through a lipid bilayer: insights from dual-resolution molecular dynamics. Soft Matter 6:3797–3808

Pal T, Jana NR (1993) Emodin (1,3,8-trihydroxy-6-methylanthraquinone): a spectrophotometric reagent for the determination of beryllium(II), magnesium(II) and calcium(II). Analyst 118:1337–1342

Parr RG, Yang W (1994) Density functional theory of atoms and molecules. Oxford University Press, Oxford

Peetla C, Stine A, Labhasetwar V (2009) Biophysical interactions with model lipid membranes: applications in drug discovery and drug delivery. Mol Pharm 6:1264–1276

Pereira CS, Lins RD, Chandrasekhar I, Freitas LCG, Hünenberger PH (2004) Interaction of the disaccharide Trehalose with a Phospholipid Bilayer: a molecular dynamics study. Biophys J 86:2273–2285

Petrache HI, Dodd SW, Brown MF (2000) Area per lipid and acyl length distributions in fluid phosphatidylcholines determined by (2)H NMR spectroscopy. Biophys J 79:3172–3192

Petrache HI, Tristram-Nagle S, Nagle JF (1998) Fluid phase structure of EPC and DMPC bilayers. Chem Phys Lipid 95:83–94

Poger D, Mark AE (2010) On the validation of molecular dynamics simulations of saturated and cis-monounsaturated Phosphatidylcholine lipid Bilayers: a comparison with experiment. J Chem Theory Comput 6:325–336

Poger D, Mark AE (2012) Lipid Bilayers: the effect of force field on ordering and dynamics. J Chem Theory Comput 8:4807–4817

Poger D, Mark AE (2013) The relative effect of sterols and Hopanoids on lipid Bilayers: when comparable is not identical. J Phys Chem B 117:16129–16140

Poger D, van Gunsteren WF, Mark AE (2010) A new force field for simulating phosphatidylcholine bilayers. J Comput Chem 31: 1117–1125

Rajarathnam K, Rösgen J (2014) Isothermal titration calorimetry of membrane proteins - progress and challenges. Biochim Biophys Acta 1838:69–77

Rand RP, Parsegian VA (1989) Hydration forces between phospholipid bilayers. Biochim Biophys Acta 988:351–376

Rissanen S, Kumorek M, Martinez-Seara H, Li YC, Jamroz D, Bunker A, Nowakowska M, Vattulainen I, Kepczynski M, Roǵ T (2014) Effect of PEGylation on drug entry into lipid Bilayer. J Phys Chem B 118: 144–151

Robinson AJ, Richards WG, Thomas PJ, Hann MM (1995) Behavior of cholesterol and its effect on headgroup and chain conformations in lipid bilayers: a molecular dynamics study. Biophys J 68:164–170

Sabín J, Prieto G, Ruso JM, Messina PV, Salgado FJ, Nogueira M, Costas M, Sarmiento F (2009) Interactions between DMPC Liposomes and the serum blood proteins HSA and IgG. J Phys Chem B 113:1655–1661

Sachs JN, Petrache HI, Woolf TB (2003) Interpretation of small angle X-ray measurements guided by molecular dynamics simulations of lipid bilayers. Chem Phys Lipid 126:211–223

Saito ST, Silva G, Pungartnik C, Brendel MJ (2012) Study of DNA–emodin interaction by FTIR and UV–Vis spectroscopy. Photochem Photobiol B 111:59–63

Schmid N, Eichenberger AP, Choutko A, Riniker S, Winger M, Mark AE, van Gunsteren WF (2011) Definition and testing of the GROMOS force-field versions 54A7 and 54B7. Eur Biophys J 40:843–856

Seddon AM, Casey D, Law RV, Gee A, Templera RH, Cesab O (2009) Drug interactions with lipid membranes. Chem Soc Rev 38:2509–2519

Sevilla P, Blanco FG, Ramos JVG, Cortés SS (2009) Aggregation of antitumoral drug emodin on Ag nanoparticles: SEF, SERS and fluorescence lifetime experiments. Phys Chem Chem Phys 11:8342–8348

Sevilla P, De-Llanos R, Domingo C, Sanchez-Cortes S, Garcia-Ramos JV (2010) SERS plus MEF of the anti tumoral drug emodin adsorbed on silver nanoparticles. In: VoDinh T, Lakowicz JR (eds) Plasmonics in biology and medicine. Proceedings of SPIE, Volume 7577, 25 - 28 January, 2010, Bellingham, USA

Seydel JK, Wiese M (2002) Drug-membrane interactions: analysis, drug distribution, modeling, vol 15. , Weinheim

Sirk TW, Brown EF, Friedman M, Sum AK (2009) Molecular binding of Catechins to biomembranes: relationship to biological activity. J Agric Food Chem 57:6720–6728

Sirka KK (2014) Separation of molecules, macromolecules and particles: principles, phenomena and processes. Cambridge University Press, New York

Smaby JM, Momsen MM, Brockman HL, Brown RE (1997) Phosphatidylcholine acyl unsaturation modulates the decrease in interfacial elasticity induced by cholesterol. Biophys J 73:1492–1505

Smondyrev AM, Berkowitz ML (1999) Structure of Dipalmitoylphosphatidylcholine/cholesterol Bilayer at Lowand high cholesterol concentrations: molecular dynamics simulation. Biophys J 77:2075–2089

Smondyrev AM, Berkowitz ML (2001) Molecular dynamics simulation of the structure of Dimyristoylphosphatidylcholine Bilayers with cholesterol, Ergosterol, and Lanosterol. Biophys J 80:1649–1658

Spoel DVD, Lindahl E, Hess B, Groenhof G, Mark AE, Berendsen HJC (2005) GROMACS: fast, flexible, and free. J Comput Chem 26: 1701–1718

Srinivas G, Anto RJ, Srinivas P, Vidhyalakshmi S, Senan VP, Karunagaran D (2003) Emodin induces apoptosis of human cervical cancer cells through poly(ADP-ribose) polymerase cleavage and activation of caspase-9. Eur J Pharmacol 473:117–125

Thomson RH (1987) Naturally occurring Quinones, vol 3. Chapman and Hall, London

Tieleman DP, Marrink SJ, Berendsen HJC (1997) A computer perspective of membranes: molecular dynamics studies of lipid bilayer systems. Biochim Biophys Acta 1331:235–270

To LV (1984) Emodin - a fungal metabolite - and the effects of Emodin on the growth of some soil microorganisms. Acta Agrar Silv Ser Agrar 23:235–242

Vargas F, Rivas C, Medrano M (2004) Interaction of Emodin, aloe-Emodin, and Rhein with human serum albumin: a fluorescence spectroscopic study. Toxicol Mech Methods 14:227–231

Vermeer LS, de Groot BL, Réat V, Milon A, Czaplicki J (2007) Acyl chain order parameter profiles in phospholipid bilayers: computation from molecular dynamics simulations and comparison with 2H NMR experiments. Eur Biophys J 36:919–931

Wang L, Lin L, Ye BJ (2006) Electrochemical studies of the interaction of the anticancer herbal drug emodin with DNA. Pharm Biomed Anal 42:625–629

Wang WH, Chung JG (1997) Emodin-induced inhibition of growth and DNA damage in the helicobacter pylori. Curr Microbiol 35:262–266

Witzke S, Duelund L, Kongsted J, Petersen M, Mouritsen OG, Khandelia H (2010) Inclusion of Terpenoid plant extracts in lipid Bilayers investigated by molecular dynamics simulations. J Phys Chem B 114:15825–15831

Xiang TX, Anderson BD (2006) Liposomal drug transport: a molecular perspective from molecular dynamics simulations in lipid bilayers. Adv Drug Deliv Rev 58:1357–1378

Yamamoto E, Akimoto T, Shimizu H, Hirano Y, Yasui M, Yasuoka K (2012) Diffusive nature of xenon anesthetic changes properties of a lipid Bilayer: molecular dynamics simulations. J Phys Chem B 116: 8989–8995

Zhang L, Hung MC (1996) Sensitization of HER-2/neu-overexpressing non-small cell lung cancer cells to chemotherapeutic drugs by tyrosine kinase inhibitor emodin. Oncogene 12:571–576

Zhou XM, Chen QH (1988) Biochemical study of Chinese rhubarb. XXII. Inhibitory effect of anthraquinone derivatives on Na+−K+−ATPase of the rabbit renal medulla and their diuretic action. Yao Xue Xue Bao 23:17–20

Zubrzycki IZ, Xu Y, Madrid M, Tang P (2000) Molecular dynamics simulations of a fully hydrated dimyristoylphosphatidylcholine membrane in liquid-crystalline phase. J Chem Phys 112:3437–3441